









Fission product yields from the $^{238}\text{U}(n, f)$ reaction at $E_n = 4.6$ MeV

A. P. D. Ramirez ^{1,*}, J. A. Silano ¹, R. C. Malone ¹, M. A. Stoyer¹, A. P. Tonchev ^{1,2}, M. E. Gooden ³, J. B. Wilhelmy³,
S. W. Finch ^{2,4}, C. R. Howell ^{2,4}, Krishichayan^{2,4} and W. Tornow ^{2,4}

¹Nuclear and Chemical Sciences Division, Lawrence Livermore National Laboratory, Livermore, California 94550, USA

²Department of Physics, Duke University, Durham, North Carolina 27708, USA

³Los Alamos National Laboratory, Los Alamos, New Mexico 87545, USA

⁴Triangle Universities Nuclear Laboratory, Durham, North Carolina 27708, USA



(Received 27 January 2023; revised 20 February 2023; accepted 21 April 2023; published 17 May 2023)

We present cumulative fission product yields from the $^{238}\text{U}(n, f)$ reaction at an incident energy of 4.6 MeV for fission products with half-lives from less than one second to several hours. We employed direct γ -ray spectroscopy to measure unseparated fission products with a conventional neutron activation analysis and a cyclic activation technique using the RAPid Belt-driven Irradiated Target Transfer System (RABITTS). Yields were determined for 78 isotopes and isomers, covering the mass range $84 \leq A \leq 148$ and the charge range from $33(\text{As}) \leq Z \leq 58(\text{Ce})$. Our experimental cumulative yields are compared to the literature and evaluated data at $E_n \approx 0.5$ MeV from ENDF/B-VIII.0 and JEFF-3.3 libraries and with theoretical models using the GEF and FREYA codes at $E_n = 4.6$ MeV.

DOI: [10.1103/PhysRevC.107.054608](https://doi.org/10.1103/PhysRevC.107.054608)

I. INTRODUCTION

Fission product yields (FPYs) are one of the most meticulously investigated observables following the nuclear fission of a heavy nucleus. An FPY is defined as the probability that a specific isotope is produced in one fission event and is generally normalized to 200% because a binary fission event yields two fragments. The knowledge of precise FPYs is vital in many areas of nuclear science and technology (e.g., reactor operations, waste storage, calculation of criticality and reactivity), stockpile stewardship, and nuclear forensics [1–3]. Fission product yield data are also of significant importance for the fundamental understanding of the fission process, including its role in the formation of heavy elements in astrophysical environments through the r -process nucleosynthesis [4]. For many of these applications, the dependence of the FPY distribution on the species of fissioning nuclide and the incident neutron energy are critical to improving the accuracy of modeling such systems. It is typical to rely on nuclear evaluation libraries such as ENDF [5], JEFF [6], and JENDL [7]. These data libraries are industry standards in nuclear physics research and nuclear applications. Unfortunately, for FPY data, these libraries are currently limited to only a few neutron energies (e.g., thermal, fission spectrum, and 14 MeV). Beyond that there is heavy dependence on theoretical predictions to provide these yields not only for a wider neutron energy range but also for a variety of fissioning nuclides [8,9]. Theoretical calculation of FPYs is the preferred approach for many applications in cases where experimental data are not available, such as in astrophysics, where nuclei of interest can

be very short lived or highly exotic and experimentally inaccessible. Recent progress in various theoretical models has led to a better understanding of the enigmatic many-body nuclear process. However, the theoretical description of fission is still far from complete. High accuracy FPY data over a broad range of masses are critically needed to provide benchmarks of theoretical calculations and as input for optimizing fission model parameters [10–12].

A considerable amount of FPY data exists for neutron-induced fission of the three major actinides (^{235}U , ^{238}U , ^{239}Pu). These data have been reported and compiled into the EXFOR experimental nuclear reaction database [13]. A widely used and well-established method for studying FPYs is the neutron activation technique where neutrons irradiate the actinide sample and the fission products are quantified using β and/or γ -ray counting or mass spectrometry. In many early measurements, the radionuclides of interest were chemically separated from the sample before counting for an accurate fission yield determination. This intermediate step between the end of target irradiation and the start of counting limits measurements to fission products with long half-lives (or large mass-chain yields). In addition, because the sample-activity losses during the radiochemical procedures are significant in many cases, this technique is mainly carried out at nuclear reactors where high fluxes and thermal cross sections can provide the necessary fission-induced activity. Also, because the sample is destroyed in the process, repeated irradiation is not possible.

In contrast, high-resolution γ -ray spectroscopy can be performed directly on the irradiated sample as a non-destructive procedure. In principle, γ rays from all fission products can be observed, although γ -ray interferences and detector characteristics limit the number of identifiable isotopes in practice.

*Corresponding author: ramirez112@llnl.gov

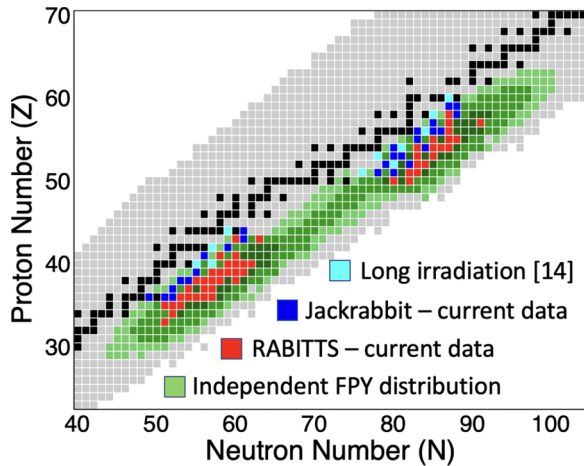


FIG. 1. Experimentally measured FPYs from the $^{238}\text{U}(n, f)$ reaction using the long-irradiation [14] (cyan squares), the Jackrabbit (blue squares), and the RABITTS (red squares) techniques. The green squares are the independent FPY distribution based on Ref. [5] while the black squares indicate the stable isotopes.

Eliminating the need for chemical separation also reduces the time between activation and decay, providing access to fission products with shorter half-lives. Since the target is not destroyed by the measurement, the cycle can be repeated many times allowing cyclic activation analysis to measure isotopes that completely decay within a few minutes.

Our LLNL-LANL-TUNL collaboration has completed a campaign to measure the energy dependence of FPYs from neutron-induced fission of ^{235}U , ^{238}U , and ^{239}Pu with E_n from 0.58 to 14.8 MeV. We have previously published data for 14 isotopes obtained using the conventional activation technique for fission products with half-lives longer than several hours in Refs. [14–18].

In the present paper, we report the cumulative FPYs from neutron-induced fission in ^{238}U at $E_n = 4.6$ MeV, including the results from the first fission yield measurements carried out with the RAPid Belt-driven Irradiated Target Transfer System (RABITTS) [19]. This system allows for measuring fission products with half-lives of a few minutes down to less than a second. We also report results using the conventional activation technique for obtaining FPYs with half-lives from a few hours down to several minutes, referred to as the “Jackrabbit” technique. These new data greatly expand our previously published FPYs in Refs. [14–18], as shown in Fig. 1, reaching fission products at the peak of the primary fission yield distribution through the RABITTS method. We describe the experimental setup, as well as the Jackrabbit and RABITTS methods in Sec. II. We then give details of the analysis procedure and present results in Sec. III followed by the conclusion in Sec. IV.

II. EXPERIMENTAL METHODS

All measurements were performed at the Triangle Universities Nuclear Laboratory (TUNL) using the 10 MV tandem Van de Graaff accelerator. The neutron beam was generated via the $^2\text{H}(d, n)^3\text{He}$ reaction by bombarding a 3 cm long gas

TABLE I. ^{238}U activation and reference foil information. The isotopic compositions of all foils are known to better than 0.02%.

Target	Diameter (mm)	Mass (mg)	Isotopic composition (%)
Thick	12.42(5)	441.9(6)	^{238}U : 99.974 ^{235}U : 0.026
FC2	12.7	0.1243(16)	^{238}U : 99.9823
FC1	12.7	0.1368(18)	^{238}U : 99.9823

cell filled with 3 atm of deuterium gas with a deuteron beam with energy $E_d = 2.43$ MeV. The gas cell was attached at the end of the beamline and was separated from the accelerator vacuum by a 6.35 μm thick Havar foil. The neutron flux was monitored using a liquid scintillation detector positioned downstream from the neutron production target at 0° relative to the incident deuteron beam direction. The neutron energy spread was determined to be approximately 360 keV full width at half maximum (FWHM) from the neutron time-of-flight spectrum measured with the liquid scintillator [14].

In this work, the Jackrabbit and RABITTS techniques, which are discussed further in the next section, were used to study the short-lived fission products with half-lives less than a few hours. Both techniques use the neutron activation method with the gas cell, activation target, and fission chamber in close proximity, with a typical separation distance of less than 3 cm. Such a compact configuration increases the neutron flux at the actinide target and the corresponding fission rate. However, the sample subtends a wide angular range in such a tight geometry, resulting in a larger neutron energy spread of 400 keV FWHM at the target position due to the intrinsic angular-energy distribution of the neutron beam.

The properties of the ^{238}U thick activation target and thin reference foils used in the dedicated dual fission ionization chamber (DFC) [14–17] are given in Table I. Recently, the masses of the thin foils were remeasured using α spectroscopy, γ -ray spectroscopy, and 2π gas proportional counting [18]. The updated masses listed in Table I were used in this work. The thick target was sealed with a 7 mg/cm² mylar tape to prevent material loss during irradiation and to catch fission products produced on the outer surface of the target.

A. Jackrabbit technique

The Jackrabbit technique employs the standard procedure for performing neutron activation analysis. It involves continuous irradiation of the activation target in the TUNL neutron time-of-flight (NTOF) room followed by γ -ray assay of the material. The target is contained in the DFC during irradiation for an accurate fission rate determination. After irradiation, the target is removed from the DFC and placed in an acrylic target holder. It is then transferred to the low-background counting facility where the induced γ -ray activity is measured by a well-shielded high-purity Germanium (HPGe) detector with 50% efficiency relative to a 3 in. \times 3 in. NaI detector. Our samples were placed 5 cm from the face of the HPGe detector using a plastic holder and rack system to ensure

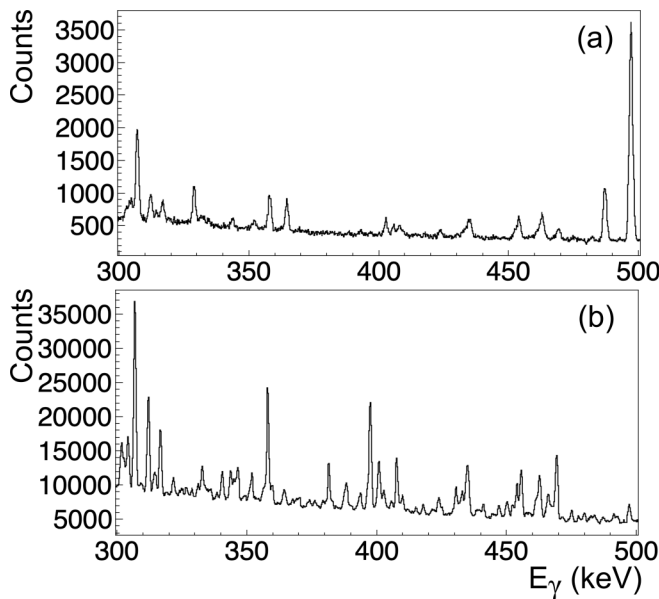


FIG. 2. γ -ray spectra obtained using the (a) Jackrabbit and (b) RABITTS techniques. The RABITTS data were taken from the 4 s irradiation and 20 s counting cycle. Many of the peaks observed in the RABITTS spectrum are from short-lived fission products that are not visible in the Jackrabbit spectrum.

reproducibility. This procedure has been discussed in detail in Ref. [14] and has been used in our long-irradiation measurements for studying fission products with half-lives over two hours [14–18]. In the Jackrabbit technique, we significantly reduced the irradiation (counting) times from days (months) to hours (weeks) to optimize the experiment for fission products with half-lives from minutes to a few hours. By doing so, we also minimized the buildup of long-lived fission products that could potentially interfere with the γ -ray lines of interest or increase the overall continuum background in the measured γ -ray spectra. An example γ -ray spectrum obtained from the Jackrabbit measurement is presented in Fig. 2(a).

An important component of the Jackrabbit technique is the utilization of the DFC. For this measurement, the DFC contained two thin ^{238}U reference foils (see Table I). During irradiation, the thick ^{238}U activation target is placed in the center of the DFC between the two reference foils. Fission fragments escaping from the reference foils are measured throughout irradiation. This provides a straightforward and precise determination of the fission rate in the thick target based on the measured fission rates in the reference foils and the ratio of the thick and thin foil masses. Since the primary activation target and the reference foils contain the same actinide, prior knowledge of the fission reaction cross sections and the absolute neutron flux is not required, removing a potential source of systematic uncertainty. We also developed a GEANT4 simulation [20] to determine the efficiency of the upstream and downstream fission chambers, including the correction for the kinematic boost from the neutron beam. For the ^{238}U fission chamber at $E_n = 4.6$ MeV, the upstream and downstream efficiencies were found to be 97.37(22)%

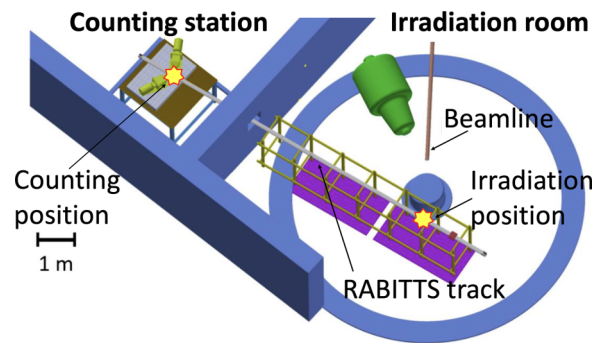


FIG. 3. A schematic diagram showing the 10 m RABITTS at TUNL. Irradiation occurs in the NTOF room and counting in the adjacent room where the counting station is setup.

and 99.29(22)%, which are consistent with previous measurements [14,16].

After neutron irradiation, the Jackrabbit method requires three to five minutes to complete the transfer of the activation target from the NTOF room to the TUNL low-background counting facility. This amount of time restricts the sensitivity of the Jackrabbit method to fission products with half-lives greater than a few minutes. For this reason, we developed RABITTS and used the cyclic activation analysis to study fission products with shorter half-lives.

B. RABITTS technique

The RAPid Belt-driven Irradiated Target Transfer System (RABITTS) was installed at TUNL to extend our FPY measurement campaign to fission products with half-lives of less than one second to a few minutes. The RABITTS allows cyclic activation analysis where the target is repeatedly irradiated by the neutron beam and then counted by γ -ray detectors. The system utilizes a stepping motor and belt-driven mechanism for transporting the target between irradiation and counting positions with extreme stability and excellent repeatability. These features are necessary for an accurate FPY determination, especially for experiments that involve hundreds or thousands of cycles in each run. The RABITTS irradiation is carried out in the NTOF room while the counting is performed in the adjacent room as shown in Fig. 3. Both rooms are separated by a thick concrete wall, where a small hole was made to insert the 10 m track and to permit passage of the target during the cyclic activation run. The length of time the sample is irradiated and counted in each cycle is chosen to improve the counting statistics, especially for the short-lived nuclides. For complete details of the RABITTS capabilities, see Ref. [19].

The compact geometry of the gas cell, the ^{238}U activation target, and the DFC at the irradiation position is illustrated in Fig. 4(a). Unlike the Jackrabbit technique, the RABITTS requires the thick ^{238}U foil to be placed outside the DFC to allow cyclic activation. The thick activation foil was held by a carbon fiber target holder and secured to a carriage that moved the target between the irradiation and counting positions. In these measurements, the ^{238}U foil was positioned about 2 cm away from the gas cell and 0.5 cm from the DFC

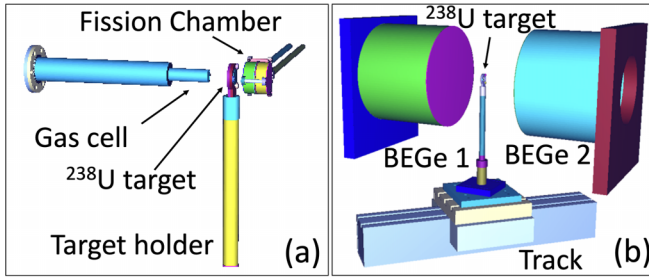


FIG. 4. MCNP models of setup at (a) irradiation position (with the gas cell, ^{238}U activation target, and dual fission chamber) and (b) counting station (with the Pb-shielded BEGe detectors and the activation target).

with their centers aligned by a telescope. A 0.5 mm thick Cd foil covered the activation target to reduce fission induced by room-scattered low-energy neutrons.

The γ -ray counting station consisted of two broad energy germanium (BEGe) detectors (60% relative efficiency) as shown in Fig. 4(b). The BEGe detectors were positioned 18 cm apart with the thick actinide target at the center. Each detector was surrounded by a 3.48 cm thick lead annulus to reduce the detection of background γ rays. While the sample was counted, the incident deuteron beam was deflected vertically by a steerer magnet located several meters upstream the gas cell and outside the NTOF room, preventing neutron production. There were also 1 mm thick Cd foils placed in front of the detectors to minimize the detection of x rays emanating from the activation foil resulting in decreased detector dead time. The absolute detector efficiency was determined using standard radioactive calibration sources covering γ -ray energies from 50 keV to 2.5 MeV. Each source was positioned at the same distance as the ^{238}U production target with identical conditions (same target holder and Cd material) as used in the FPY measurement. The experimental and MCNP calculated absolute detector efficiency for one of the BEGe detectors and the corresponding energy resolution (FWHM) as a function of γ -ray energy are shown in Fig. 5.

Cyclic activation was performed with three different cycle-time structures to optimize the FPY measurement for various half-lives. The cycle times are given in Table II. The transit time between the irradiation and counting positions was about 1.04 s for all runs. Typically, the cyclic activation was performed for 12 hours at a time. Then the sample was counted continuously for another 12 hours overnight with no neutron beam. This served several purposes: (i) the cool-down period minimized the build-up of long-lived fission products in the sample; (ii) it allowed counting of natural backgrounds in the sample; and most importantly, (iii) it allowed counting of fission products with half-lives on the order of a few hours for determination of the neutron flux (discussed in Sec. III C).

III. DATA ANALYSIS AND RESULTS

Neutron activation analysis is a well-established technique that involves the measurement of delayed γ rays following neutron irradiation. Due to the complex γ -ray spectrum generated during the fission reaction (see Fig. 2), high-resolution

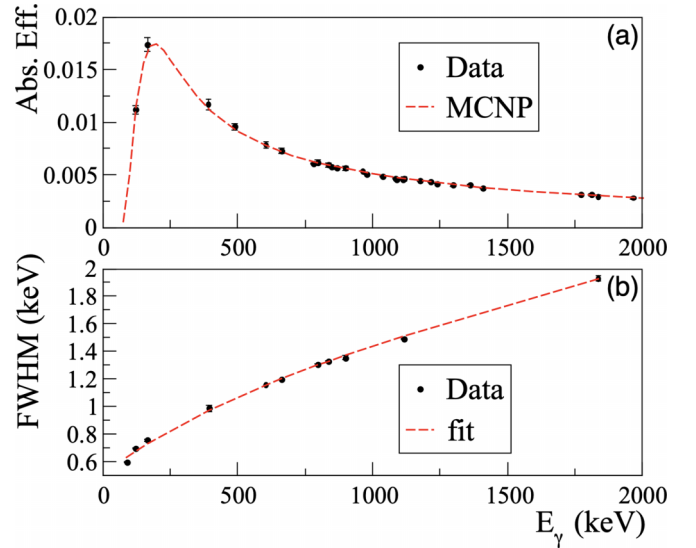


FIG. 5. (a) Detector efficiency and (b) energy resolution for one of the BEGe detectors positioned 9 cm away from the activation target. Data points are measured values while the curve in (a) is from MCNP simulation and that in (b) is fit to data using the analytical expression $f(E_\gamma) = [0.522^2 + 0.042^2 E_\gamma + (2.52 \cdot 10^{-4})^2 E_\gamma^2]^{1/2}$.

γ -ray spectroscopy was utilized to identify fission products according to their known decay transitions and to determine the induced activity of each fission product. Additionally, the decay curve of each γ -ray line was fitted using the known half-life to confirm the isotopic identification. We have applied these analysis methods in our long-irradiation and Jackrabbit measurements, which have been explained in great detail in Ref. [14]. We used the same analysis procedure for the RABITTS measurements with slight modifications to account for the cyclic activation process. The procedures specific to our RABITTS measurements have also been described in Ref. [19]. Here, we elaborate on the RABITTS analysis for obtaining cumulative FPYs.

During a cyclic activation run, data were acquired in list mode, which records the pulse-height and timestamp of each event. Data were processed offline, where the pulse-height spectra were calibrated to accurately determine the γ -ray energies, and the timestamp was used to chronologically sort events and then group them depending on what part of the cycle they occurred: during irradiation (or *exposure*, labeled t_e), during transit (or *decay*, labeled t_d), or during counting (or *measurement*, labeled t_m). After categorization, the events were histogrammed using appropriate time bins for the peaks of interest.

A portion of a BEGe detection rate as a function of time is shown in Fig. 6(a). For further data processing, we merged the spectra from all n cycles to produce a single-cycle “summed spectrum” as shown in Fig. 6(b). The relevant events were those during the counting period t_m when the activation target was being counted by the BEGe detectors ([see Fig. 2(b) for example RABITTS γ -ray spectrum]). The exponential decay of the BEGe counting rate indicates events from the decay of the short-lived fission products in the target. It is also worth

TABLE II. Information about the various activation cycles used in this work. Total time does not include the overnight runs.

Irradiation time (s)	Counting time (s)	Number of cycles	Total time (hr)
4	20	4053	29.3
10	60	1054	21.1
60	300	194	19.5

mentioning that in the summed spectrum, the BEGe activity was relatively high during the irradiation period t_e even though the target was not in front of the BEGe detectors. This suggests that neutrons leak from the NTOF room to the counting station during irradiation and highlights the importance of deflecting the beam during counting.

When a peak in a γ -ray spectrum has been confirmed to originate from a specific fission product, its activity after neutron irradiation at time t_0 can be evaluated based on the number of γ rays detected during the counting period. The activity $A(t_0)$ can be obtained by fitting the decay curve. An example is shown in Fig. 7. For the decay of a single radionuclide, the cumulative yield can be determined using the expression

$$\text{FPY} = \frac{\lambda N_\gamma}{F_T I_\gamma \epsilon_\gamma (1 - e^{\lambda t_e})(e^{\lambda t_d})(1 - e^{\lambda t_m})} \mathcal{G} \prod_k C_k, \quad (1)$$

where λ is the decay constant for the fission product, N_γ is the number of γ -rays in a photopeak (summed over n cycles for cyclic activation), F_T is the fission rate in the target, I_γ is the γ -ray intensity, ϵ_γ is the full-energy peak efficiency of the detector for the γ -ray energy of interest, and C_k are

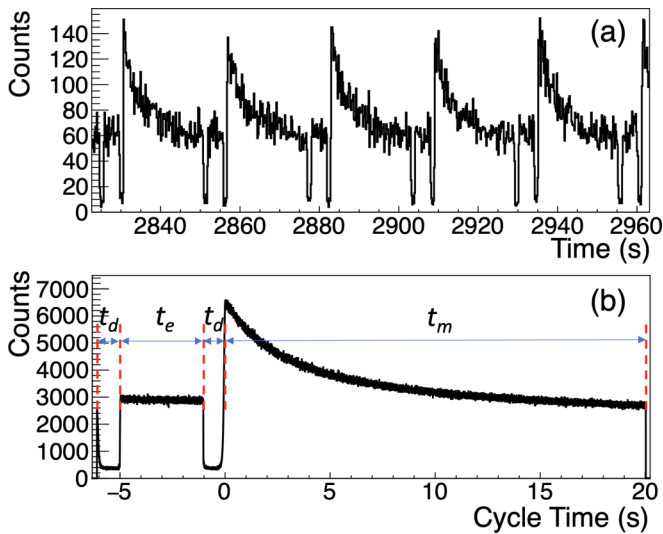


FIG. 6. (a) A section of the timestamp histogram for one of the BEGe detectors showing the detection rate as a function of time from the 4 s/20 s cycle run. (b) Single-cycle ‘‘summed spectrum’’ generated by merging all cycles from the 4 s/20 s data. The labeled time intervals are the transit decay time t_d , the irradiation time t_e , and counting time t_m .

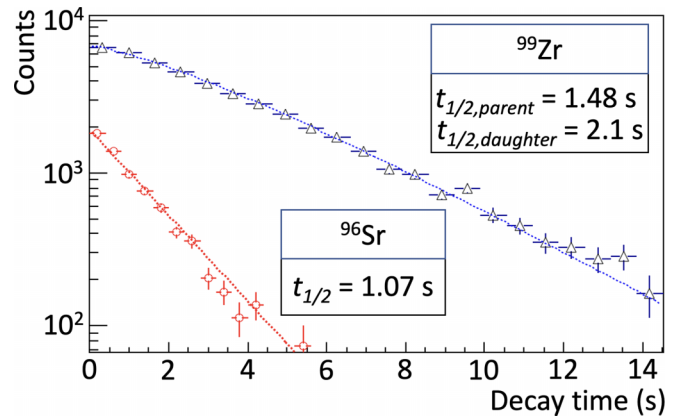


FIG. 7. Example decay curves observed for ^{96}Sr (red circles) and ^{99}Zr (blue triangles) using the 809 and 469 keV γ rays, respectively. Decay curves were fitted to the data by fixing the half-life parameter to values from ENSDF [23]. See text for details.

correction factors accounting for the beam flux fluctuation, γ -ray attenuation, off-energy neutrons, isotopic impurities, and γ -ray coincidence summing. For conventional activation analysis, the factor $\mathcal{G} = 1$, and for cyclic activation it is given by

$$\mathcal{G} = \frac{(1 - e^{-\lambda T})}{n} - \frac{(1 - e^{-\lambda T})^2}{e^{-\lambda T}(1 - e^{-n\lambda T})}, \quad (2)$$

where T is the time for one complete cycle ($T = t_e + 2t_d + t_m$) and n is the total number of cycles. A detailed derivation of Eq. (2) describing cyclic activation analysis is given in Refs. [21,22]. F_T is determined from the DFC in the Jackrabbit analysis and known FPYs in RABITTS (see Sec. III C). The nuclear structure information, such as the half-life $t_{1/2}$, the γ -ray energy E_γ , and the γ -ray intensity I_γ , have been taken from the evaluated nuclear structure database (ENSDF) [23].

In a fission reaction, decay chains may involve consecutive β decays where a radionuclide decays to another unstable nuclide. In order to accurately calculate a cumulative FPY, it is necessary to incorporate the feeding due to the decay of the precursor nuclides resulting in an increase in the daughter fission product’s activity. One can solve the Bateman equations [24] for the activities and cumulative yields during irradiation. For a chain involving the decay of parent and daughter fission products, their corresponding activities during irradiation follow the expressions

$$A_p(t_0) = f_p(1 - e^{-\lambda_p t_e}) \mathcal{G}_p \quad (3)$$

and

$$\begin{aligned} A_d(t_0) = & (f_d + f_p)(1 - e^{-\lambda_d t_e}) \mathcal{G}_d \\ & + \frac{f_p \lambda_d}{\lambda_p - \lambda_d} (e^{-\lambda_p t_e} - e^{-\lambda_d t_e}) \mathcal{G}_d \\ & + \frac{\lambda_d}{\lambda_p - \lambda_d} A_p(t_0) (1 - e^{-\lambda_p t_e}) [\mathcal{G}_d - \mathcal{G}_p]. \end{aligned} \quad (4)$$

Here, the parameters with subscripts p and d represent the parent and daughter, respectively, and $f = \text{FPY} \times F_T$. Similarly, the Bateman equation for the measured activity of the

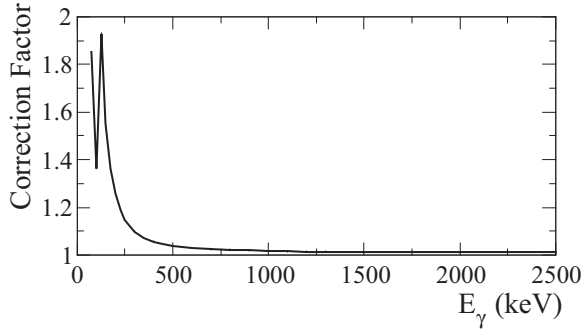


FIG. 8. Self-absorption and geometry correction factor as a function of γ -ray energy for the thick ^{238}U activation target.

daughter nuclide during the counting period is given by

$$A_d(t_m) = \frac{\lambda_d}{\lambda_p - \lambda_d} A_p(t_0 + t_d) (e^{-\lambda_d t_m} - e^{-\lambda_p t_m}) + A_d(t_0 + t_d) e^{-\lambda_d t_m}. \quad (5)$$

An example decay curve showing the decay of a daughter nuclide ^{99}Zr ($t_{1/2} = 2.10$ s) and parent nuclide ^{99}Y ($t_{1/2} = 1.48$ s) is shown in Fig. 7. Because these nuclei have comparable half-lives, the decay curve of ^{99}Zr is influenced by the decay of ^{99}Y and must therefore be included in the fit using Eq. (5). The activities $A_p(t_0)$ and $A_d(t_0)$ obtained from the fit were then substituted into Eqs. (3) and (4) to determine the cumulative FPY of ^{99}Zr . We generally employed this procedure when the half-life of the parent nuclide is 10% or longer than the half-life of the daughter nuclide. Otherwise, we assume the parent population has decayed into the daughter nuclide and Eq. (1) can be used.

A. Corrections

As indicated in the previous section, an accurate FPY determination requires several corrections to Eq. (1) or (5). All correction factors briefly described in this section apply to both the Jackrabbit and RABITTS data.

- (i) *Self-attenuation and geometry corrections.* This correction accounts for the different geometry and absorption of γ rays in the calibration source and the activation sample. The calibration source was a point source enclosed in a plastic disk, while the activation sample was a thin disk composed of uranium. The geometric effect is due to the difference in the effective solid angle subtended by the γ -ray detector relative to the activation target and calibration source. The absorption of γ rays in the calibration source and activation sample differ because of their different geometries and materials. This effect can be significant, especially for photon energies below 200 keV. To account for these effects, we developed an MCNP simulation [25] to determine the combined self-absorption and geometric correction factors, which are displayed in Fig. 8. For our counting configuration, self-absorption dominates this correction with the geometry effects contributing only about 1% or

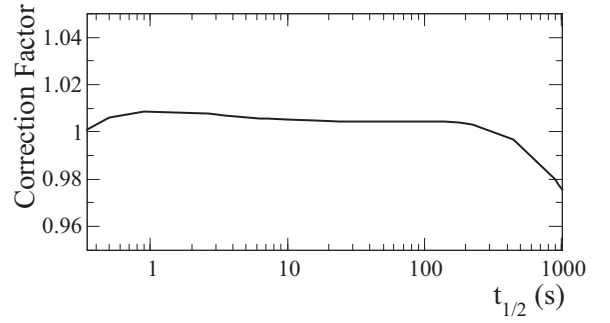


FIG. 9. Neutron beam flux fluctuation correction factor as a function of $t_{1/2}$ specific for the present RABITTS data with 4 s/20 s cycle time.

less. Results obtained via MCNP simulations were in good agreement with analytic calculations using photon-attenuation values from the NIST XCOM database [26].

- (ii) *Beam flux fluctuation correction.* The cyclic activation equations given in the previous section were derived assuming a constant neutron beam flux. However, the neutron beam flux varied slightly over time. To correct for these variations, a numerical code was written in ROOT/C++ in order to model the activity of an isotope (specified by its half-life) for the entire experimental run including the overnight counting. The code requires the neutron monitor data measured by the liquid scintillation detector positioned downstream of the activation target to count the relative beam flux during the experiment. Details for this procedure have been thoroughly discussed in our previous work [19]. An example of the beam flux fluctuation corrections as a function of half-life is shown in Fig. 9.
- (iii) *Coincidence summing correction.* Coincidence summing can occur when a decaying nuclide emits a cascade of γ rays. When two or more γ rays deposit energy in the detector but cannot be resolved in time, the total energy acquired may result in a gain or loss of counts under the photopeak of interest. The coincidence summing effects depend primarily on the decay scheme of the nuclide, as well as the counting geometry, such as the detector dimensions and the distance from the sample to the detector. In order to account for these effects, we developed the code CADETS (CAscade DETection Summing) for calculating the summing correction factor based on the prescriptions described in Refs. [27,28]. The CADETS code requires the decay scheme information of the nuclide and the photopeak and total BEGe detection efficiencies as inputs. The former was taken from the ENSDF library [23], while the latter were calculated using the MCNP simulation [25]. The MCNP detector geometry was optimized by comparing the simulated photopeak efficiency with experimental values as shown in Fig. 5. When good agreement is achieved, we then calculate the total efficiency using the same geometry. Typical

TABLE III. Cumulative FPYs from neutron-induced fission of ^{238}U at $E_n = 4.6$ MeV. These yields are measured using the Jackrabbit technique and encompass half-lives from 10 min to 20 h. γ rays with * include another γ -ray line originating from the same isotope that cannot be resolved in the peak fitting analysis. The γ -ray intensity is the sum of both γ -ray lines.

Nuclide	E_γ (keV)	Intensity (%)	$T_{1/2}$	FPY $\pm \sigma_T$ (σ_{\min}) (%)	ENDF/B-VIII.0 (%)	JEFF-3.3 (%)
^{85m}Kr	151.20	75.2(5)	4.480(8) h	$0.88 \pm 0.08(0.08)$	0.74(1)	0.80(13)
^{87}Kr	402.59	50(3)	76.3(5) min	$1.56 \pm 0.12(0.08)$	1.63(3)	1.66(9)
^{88}Kr	2392.11	34.6(16)	2.825(19) h	$1.99 \pm 0.15(0.11)$	2.03(6)	2.22(11)
^{89}Rb	1031.92	63(3)	15.32(10) min	$3.18 \pm 0.22(0.15)$	2.76(6)	3.02(8)
	1248.14	46(3)	15.32(10) min	$3.44 \pm 0.34(0.24)$	2.76(6)	3.02(8)
^{91}Sr	1024.3	33.5(11)	9.65(6) h	$3.68 \pm 0.20(0.14)$	4.04(8)	4.21(14)
^{92}Sr	1383.93	90(6)	2.611(17) h	$4.15 \pm 0.30(0.09)$	4.31(12)	4.40(16)
^{94}Y	918.74	56(3)	18.7(1) min	$5.01 \pm 0.33(0.17)$	4.61(18)	5.05(20)
^{97}Nb	657.94	98.23(8)	72.1(7) min	$5.60 \pm 0.14(0.11)$	5.56(6)	5.73(7)
^{101}Mo	*505.92	11.98(29)	14.61(3) min	$5.74 \pm 0.57(0.55)$	6.21(37)	6.42(31)
^{104}Tc	358	89(3)	18.3(3) min	$5.09 \pm 0.23(0.12)$	5.04(10)	4.64(100)
^{105}Ru	*469.35	19.14(21)	4.439(11) h	$3.52 \pm 0.21(0.20)$	4.05(11)	3.73(16)
^{129}Sb	812.97	48.2(8)	4.366(26) h	$0.77 \pm 0.08(0.08)$	1.01(16)	0.50(3)
^{131}Te	149.72	68.8(4)	25.0(1) min	$3.14 \pm 0.17(0.16)$	3.07(9)	3.11(9)
^{131}Sb	943.41	47.1(24)	23.03(4) min	$3.89 \pm 0.27(0.18)$	3.25(13)	3.30(9)
^{133}I	529.87	87.0(23)	20.83(8) h	$7.14 \pm 0.32(0.23)$	6.76(433)	6.77(24)
^{134}Te	180.89	18.3(8)	41.8(8) min	$6.66 \pm 0.51(0.40)$	6.85(19)	6.79(62)
	210.47	22.7(13)	41.8(8) min	$6.92 \pm 0.50(0.32)$	6.85(19)	6.79(62)
^{134}I	847.03	96(3)	52.5(2) min	$7.23 \pm 0.29(0.13)$	7.60(46)	6.84(62)
	884.09	65.1(23)	52.5(2) min	$7.42 \pm 0.45(0.32)$	7.60(46)	6.84(62)
^{135}Xe	249.79	90(3)	9.14(2) h	$6.87 \pm 0.28(0.12)$	6.97(7)	6.42(24)
^{138}Xe	258.41	34.1(13)	14.14(7) min	$5.70 \pm 0.36(0.26)$	5.70(16)	6.00(19)
	1768.26	18.1(7)	14.14(7) min	$5.86 \pm 0.55(0.49)$	5.70(16)	6.00(19)
	2015.82	13.3(5)	14.14(7) min	$5.87 \pm 0.65(0.60)$	5.70(16)	6.00(19)
^{138}Cs	462.8	30.8(7)	32.5(2) min	$6.69 \pm 0.36(0.30)$	5.75(16)	6.02(19)
	1009.78	29.8(6)	32.5(2) min	$7.04 \pm 0.40(0.36)$	5.75(16)	6.02(19)
	1435.77	76.3(5)	32.5(2) min	$6.68 \pm 0.25(0.22)$	5.75(16)	6.02(19)
^{139}Ba	165.86	23.7(4)	82.93(9) min	$6.81 \pm 0.31(0.26)$	5.67(11)	5.78(27)
^{141}Ba	190.33	44.8(23)	18.27(7) min	$5.19 \pm 0.33(0.17)$	5.34(32)	5.79(34)
	343.67	15.1(8)	18.27(7) min	$6.09 \pm 0.54(0.42)$	5.34(32)	5.79(34)
^{142}Ba	255.3	20.6(8)	10.6(2) min	$5.09 \pm 0.45(0.40)$	4.58(18)	4.84(21)
	1078.7	11.5(5)	10.6(2) min	$5.43 \pm 0.80(0.76)$	4.58(18)	4.84(21)
^{142}La	641.29	47.4(5)	91.1(5) min	$4.97 \pm 0.22(0.19)$	4.59(9)	4.84(21)
	2397.8	13.3(3)	91.1(5) min	$4.62 \pm 0.31(0.28)$	4.59(9)	4.84(21)
	2542.7	10.0(3)	91.1(5) min	$4.64 \pm 0.36(0.31)$	4.59(9)	4.84(21)
^{146}Ce	218.23	19.5(5)	13.49(16) min	$2.66 \pm 0.32(0.31)$	3.45(10)	3.58(16)
	316.74	55.3(14)	13.49(16) min	$3.40 \pm 0.20(0.17)$	3.45(10)	3.58(16)
^{146}Pr	453.86	46(3)	24.09(10) min	$3.88 \pm 0.38(0.27)$	3.45(5)	3.58(16)
	1524.78	15(1)	24.09(10) min	$2.85 \pm 0.33(0.27)$	3.45(5)	3.58(16)
^{147}Pr	577.9	14.1(14)	13.44(10) min	$3.46 \pm 0.59(0.48)$	2.59(7)	2.66(4)

summing correction factors for these measurements were found to be less than 4%.

(iv) *Isotopic impurity correction.* If fissioning nuclei other than the actinide of interest are present in the sample, they contribute fission products and these must be subtracted. For this work, the ^{238}U sample was pure enough that the correction was negligible (see Table I).

(v) *Off-energy neutron correction.* Depending on the beam energy and neutron production method, neutrons can interact at energies other than the main energy of interest. These off-energy neutrons can induce fission and produce fission product yields that

must be accounted for. The off-energy neutrons in the TUNL NTOF room have been extensively studied using pulsed beams at different incident neutron energies [16]. When producing neutrons at 4.6 MeV employing the $^2\text{H}(d, n)^3\text{He}$ reaction, these backgrounds were limited and no correction was needed.

B. Jackrabbit results

Our cumulative fission product yields measured using the Jackrabbit technique for the $^{238}\text{U}(n, f)$ reaction at $E_n = 4.6$ MeV are summarized in Table III. We identified 27 radionuclides with half-lives between 10 min and 20 h. They are

TABLE IV. Principal sources of uncertainties and their estimated fractional values given in percent. Values in parenthesis apply to RABITTS data that are different from the Jackrabbit data.

Source of Uncertainty	Magnitude (in %)
Photopeak area	1.1–13.8 (15)
FC reference foil masses	1.3
Fission chamber counts	<0.2
γ -ray absorption	0.2
Neutron flux correction	1.3
Fission chamber stability	1.5
γ -ray emission probability	0.2–6.7 (30)
HPCe detector efficiency	0.8–2.0

generally comprised of nuclides that are two to three nuclear charges from the β -stability line. Hence, they need two to three successive β decays to reach the last stable member of the corresponding isobaric chain. For several of these isotopes, multiple FPY values were determined by analyzing different γ -ray lines from the same isotope. Generally, these yields vary within the quoted total uncertainty, except for ^{141}Ba , ^{146}Ce , and ^{146}Pr . A majority of the photopeak areas had uncertainties on the order of 1–5% and only for a limited number were the uncertainties larger, resulting in the range given in Table IV. The statistical uncertainty also dominates

the total FPY uncertainty, except for ^{92}Sr where its relative γ -ray intensity uncertainty is 6.7% [23]. In Table III, we report the total uncertainty σ_T and the reduced uncertainty σ_{min} . The total uncertainty combined the statistical and systematic uncertainties in quadrature. The reduced uncertainty excludes the systematic uncertainties that are correlated between different measurements (e.g., detector efficiency, γ -ray intensities; see Ref. [14] for more details). In this paper, the number in parentheses after the value of a quantity is the absolute uncertainty in the value, unless otherwise specified.

The comparisons between our Jackrabbit data and evaluated values from the ENDF-VIII.0 [5] and JEFF-3.3 [6] libraries and theoretical models are shown in Figs. 10(a) and 11(a), respectively. Since there is no evaluated FPY data at $E_n = 4.6$ MeV, we employed the nearest available data with a neutron energy of about 0.5 MeV. For our FPY data, the isotopes with more than one yield were averaged by computing their weighted mean with an average uncertainty. Generally, excellent agreement is observed between our data and the evaluated values, particularly with the JEFF-3.3 library, although a few heavy fission products have yields slightly larger than the evaluation. Also, it is noticeable that the uncertainty of the ^{133}I yield from ENDF/B-VIII.0 is significantly larger than our experimental yield and the JEFF-3.3 value.

We also compared our cumulative yields with existing literature data. Based on the EXFOR database, there are only

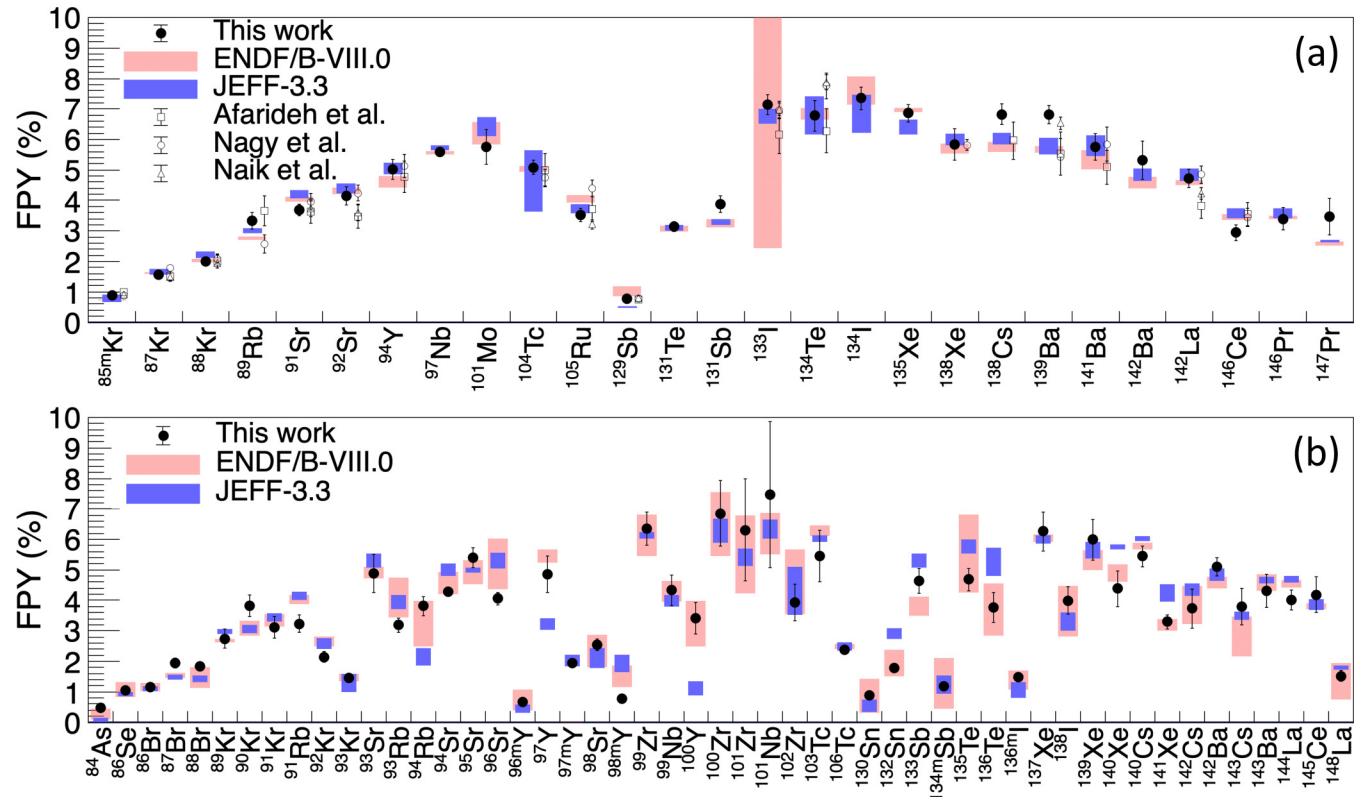


FIG. 10. Comparison of our measured cumulative yields for the $^{238}\text{U}(n, f)$ reaction (solid points) with (a) the Jackrabbit and (b) RABITTS methods at $E_n = 4.6$ MeV and the evaluated data from ENDF/B-VIII.0 [5] (red bands) and JEFF-3.3 [6] (blue bands) libraries at $E_n \approx 0.5$ MeV. Literature data from Ref. [29] at $E_n = 3.9$ MeV (open circle), Ref. [30] at $E_n = 4.78$ MeV (open square), and Ref. [31] at $E_n = 3.72$ MeV (open triangle) are also plotted and compared with the present data.

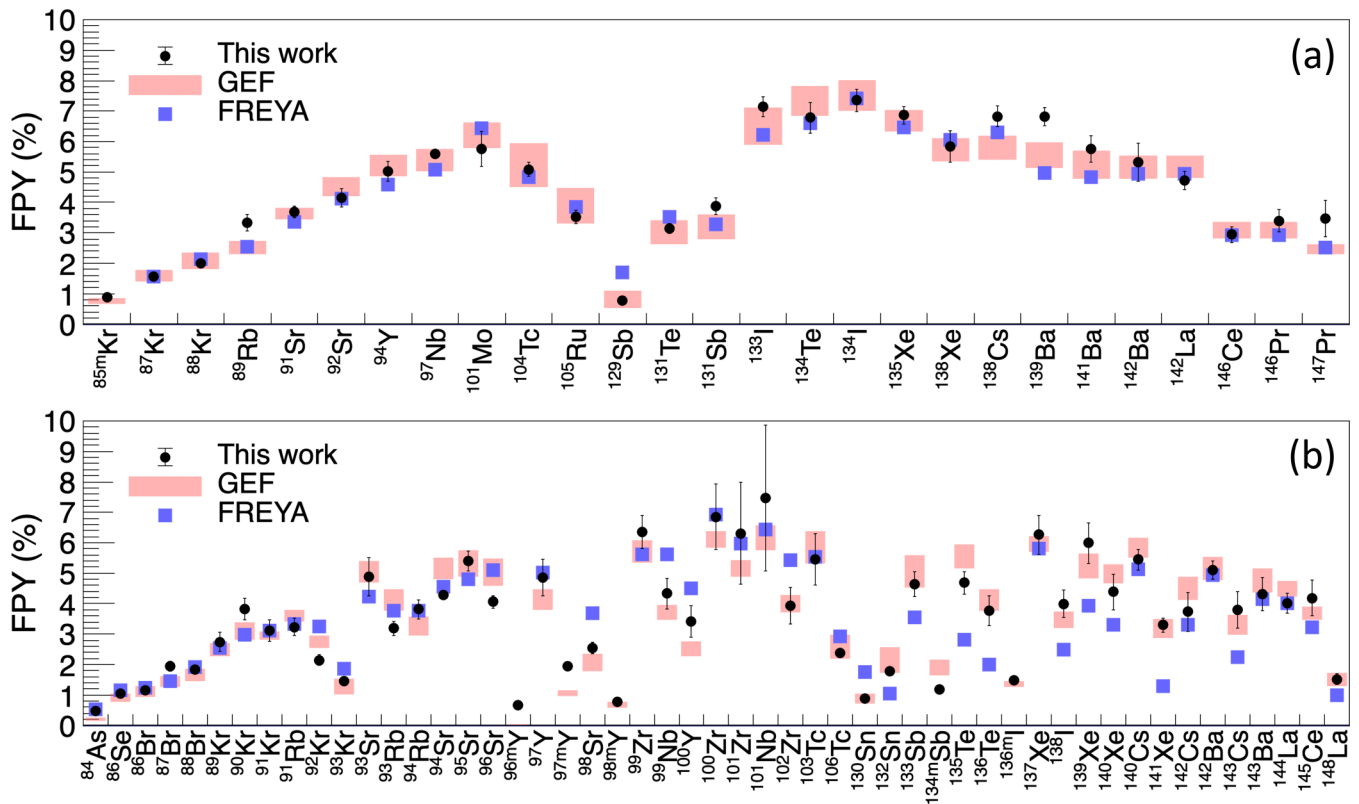


FIG. 11. Comparison of our measured cumulative yields for the $^{238}\text{U}(n, f)$ reaction (solid points) using the (a) Jackrabbit and (b) RABITTS methods with calculated yields from GEF [34] (red bands) and FREYA (blue bands) [35,36] codes.

a few available data for the $^{238}\text{U}(n, f)$ reaction with neutron energy near 4.6 MeV. These include the data by Nagy *et al.* [29], Afarideh *et al.*, [30], and Naik *et al.* [31], as well as our previous long-irradiation work in Refs. [14,18]. A comparison between the current Jackrabbit yields with literature data is also shown in Fig. 10(a). The experimental FPYs agree with each other, with only a few that appear to vary beyond the quoted total uncertainty.

C. RABITTS flux determination

Obtaining the fission rate in the sample using the RABITTS technique is not as straightforward as the Jackrabbit technique because the thick activation target is located outside the dual fission chamber. The fission rate, which contains the unknown neutron flux information, acts as the overall scaling factor to convert the relative RABITTS yields to absolute values. Our approach involves using the Jackrabbit data as reference yields FPY_{ref} that we equate to the RABITTS yields since both are measured at the same incident neutron energy. We use the Jackrabbit results as a measure of the number of γ rays detected per fission in the thick target. Then the fission rate in the RABITTS experiment can be determined from the fission rate in the Jackrabbit experiment as

$$F_{T,\text{RABITTS}} \propto F_{T,\text{Jackrabbit}} \frac{N_{\gamma,\text{RABITTS}}}{N_{\gamma,\text{Jackrabbit}}}. \quad (6)$$

It must be pointed out that the resulting fission rate F_T involves ratios of the γ -ray intensities and so uncertainties in those parameters do not impact the final result. The uncertainties in the half-lives partially cancel and therefore are also negligible.

Among the isotopes presented in Table III, the ^{92}Sr isotope provides an excellent reference candidate as the 1384 keV transition is relatively free from interfering γ rays with a convenient half-life of 2.61 h and a significant γ -ray intensity of 90(6)%. As already mentioned, the uncertainty of the intensity does not affect the uncertainty of the resulting fission rate. For this flux determination, we used the overnight data when the activation target was counted for about 12 h with no neutron beam irradiation. This allows the long-lived fission products to decay, reducing their potential interference with the short-lived products. The overnight counting immediately follows after a 12 h in-beam RABITTS run. In addition to ^{92}Sr , we have included a few more reference isotopes with their calculated fission rates shown in Fig. 12. The average fission rates from different activation cycles are given by $11410(168) \text{ s}^{-1}$, $9375(183) \text{ s}^{-1}$, and $9217(152) \text{ s}^{-1}$ for the 4 s/20 s, 10 s/60 s, and 60 s/300 s cycle times, respectively.

An MCNP calculation was also performed to estimate the fission rate in the thick target. Details on using this approach to determine the neutron flux have been provided in Ref. [19]. The MCNP calculated neutron flux ratios $\frac{\text{thick}}{\text{FC2}}$ and $\frac{\text{thick}}{\text{FC1}}$ were found to be 2.536(54) and 3.074(72) for the 4 s/20 s cycle run and 1.817(34) and 2.380(48) for the 10 s/60 s and 60 s/300 s cycle runs, respectively. The 10 s/60 s

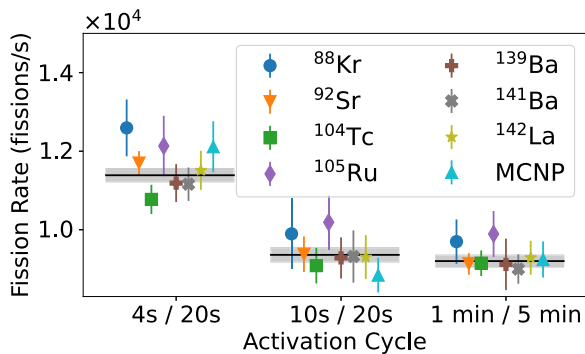


FIG. 12. Estimated fission rates for the RABITTS run with 4 s/20 s, 10 s/60 s, and 60 s/300 s cycles. The RABITTS yields for the listed isotopes were obtained from the overnight counting. The gray bands represent the average fission rate with uncertainty for each cycle. The FPY_{ref} values used to calculate these fission rates are from the Jackrabbit data.

and 60 s/300 s measurements were done consecutively with the same target and fission chamber configuration, which explains the nearly identical neutron flux ratios, while the 4 s/20 s cycle was performed at a later time with a slightly different configuration. During the RABITTS experiments, the upstream [downstream] fission chambers recorded 18429 [12522], 14372 [12528], and 16541 [14270] total numbers of fissions for the 4 s/20 s, 10 s/60 s, and 60 s/300 s cycle times, respectively. From these MCNP calculated ratios, the total number of fissions measured in the DFC, and the masses of the reference and thick ^{238}U foils given in Table I, we can then calculate the fission rates in the thick target. These values are also plotted in Fig. 12. Both approaches provide very consistent fission rates. In our RABITTS analysis, we only used the average experimental fission rates from the overnight data for normalizing our relative FPYs to absolute values.

D. RABITTS results

Using the 10 m track RABITTS, we collected data using three different activation cycles specified in Table II. The cumulative yields obtained from the RABITTS measurements are listed in Table V. A total of 51 unique radionuclides and isomers have been identified. These are typically located five or fewer nuclear charges away from the β -stability line. As with the Jackrabbit data, several of the isotopes have multiple FPY values that have been determined by analyzing different γ -ray lines from the same isotope.

Wherever possible, we compared FPYs measured with the Jackrabbit method to those obtained with the RABITTS technique to confirm consistency between the two data sets. Since each method is sensitive to a different range of FPY half-lives, only a few isotopes could be measured with both methods. One example is the 255 keV γ -ray line from ^{142}Ba which has a half-life accessible to both techniques. The measured Jackrabbit and RABITTS FPYs for this isotope are listed in Tables III and V, and both are in excellent agreement. Another example is the 1384 keV transition from ^{92}Sr . Despite its long half-life of 2.71 h, we were able to deduce the ^{92}Sr FPY from the 60 s/300 s cycle RABITTS data because its γ -ray line

does not suffer from significant interference. The RABITTS yield of 3.99(29)% is in agreement with the Jackrabbit yield of 4.15(30)%.

Our RABITTS cumulative yields are compared with the ENDF/B-VIII.0 [5] and JEFF-3.3 [6] evaluations in Fig. 10(b). Here, each RABITTS FPY was taken from the weighted average over all FPYs obtained from different cycles and from individually analyzed γ -ray lines. It is immediately noticeable that the RABITTS data generally have larger uncertainties than the Jackrabbit results (see also Table V). The uncertainties stemming from the γ -ray intensity dominate most of these large-uncertainty RABITTS FPYs. In several cases, the γ -ray intensity uncertainties are larger than 10% with a few above 20% [e.g., $E_\gamma = 205.7$ and 276.1 keV from ^{101}Zr and ^{101}Nb have I_γ of 6.1(15)% and 21(6)%, respectively]. In addition, overlapping peaks in the γ -ray spectrum due to transitions from many decaying short-lived isotopes in the RABITTS measurements contribute to increasing uncertainties of the photopeak area (see Table IV). These interfering peaks are accounted for in the peak fitting procedure where the error propagation includes uncertainties from the estimated main peak area, the background, and the overlapping peaks.

As can be seen in Fig. 10(b), our FPYs satisfactorily compare with evaluations, although it is noticed that the evaluated yields from ENDF/B-VIII.0 and JEFF-3.3 libraries are not as consistent as observed for the longer-lived fission products. Moreover, for many of these short-lived radionuclides, the uncertainties for their FPYs are relatively large. This can be attributed to the way the fission product yields are calculated in each library. Evaluated FPYs are based on experimental data from long-lived fission products near the end of the isobaric chains. Evaluated FPYs for short-lived fission products are extrapolated from the long-lived FPY data using the charge distribution model in which a Gaussian distribution is assumed for the yields that belong to an isobaric chain [32,33]. Therefore, it is important to provide experimental data for short-lived fission products to supplement the evaluation and improve the FPY description.

The comparisons of our measured cumulative yields for the $^{238}\text{U}(n, f)$ reaction using the (a) Jackrabbit and (b) RABITTS methods and calculated yields from theoretical models using the GEF [34] and FREYA [35,36] codes are shown in Fig. 11. The default GEF and FREYA calculations show very good agreement with our Jackrabbit cumulative FPYs, as shown in Fig. 11(a). However, both models underestimate the ^{89}Rb , ^{139}Ba , and ^{147}Pr FPYs. As both codes use semiempirical models, this demonstrates the need for additional high-precision energy-dependent FPY data. GEF calculations show that the long-lived nuclides, such as the ones obtained by the Jackrabbit method, are produced mainly by the decay of their precursors and not so much directly by fission. Within uncertainty, this prediction is confirmed by our experimental results shown in Tables III and V when one compares FPYs from two consecutive decays in an isobaric chain.

A summary of isotopes for which we have measured the FPYs has been shown in Fig. 1. The Jackrabbit, RABITTS, and our previously published long-lived FPYs [14] are highlighted on the nuclear chart and the FPYs for the $^{238}\text{U}(n, f)$ reaction at $E_n = 0.5$ MeV from the ENDF/B-VIII.0 evalua-

TABLE V. Fission product yields from neutron-induced fission of ^{238}U at $E_n = 4.6$ MeV. These yields are measured using the RABITTS technique and encompass half-lives from about 0.6 s to 10 min. γ rays with * include another γ -ray line originating from the same isotope that cannot be resolved in the peak fitting analysis. The γ -ray intensity is the sum of both γ -ray lines.

Nuclide	E_γ (keV)	Intensity (%)	$T_{1/2}$	FPY $\pm\sigma_T$ (σ_{\min}) (%)	ENDF/B-VIII.0 (%)	JEFF-3.3 (%)
^{84}As	1454.55	89(8)	4.02(3) s	$0.48 \pm 0.05(0.01)$	0.27(17)	0.08(7)
^{86}Se	2441.1	43(5)	14.3(3) s	$1.05 \pm 0.13(0.05)$	1.07(25)	0.93(7)
^{86}Br	1564.6	62(5)	55.1(4) s	$1.16 \pm 0.11(0.06)$	1.16(13)	1.10(8)
^{87}Br	1419.71	22.0(15)	55.65(13) s	$1.96 \pm 0.16(0.10)$	1.54(9)	1.47(8)
^{88}Br	775.28	62.5(38)	16.34(8) s	$1.85 \pm 0.12(0.04)$	1.48(34)	1.43(11)
^{89}Kr	220.95	20.1(17)	3.15(4) min	$2.62 \pm 0.38(0.31)$	2.67(5)	2.97(8)
	586.03	16.7(14)	3.15(4) min	$2.80 \pm 0.26(0.10)$	2.67(5)	2.97(8)
^{90}Kr	539.49	30.8(25)	32.32(9) s	$3.94 \pm 0.40(0.21)$	3.08(25)	3.06(14)
	1118.69	39(3)	32.32(9) s	$3.77 \pm 0.31(0.09)$	3.08(25)	3.06(14)
^{91}Kr	108.79	43.5(35)	8.57(4) s	$3.12 \pm 0.36(0.10)$	3.35(20)	3.45(13)
^{91}Rb	2564.19	12.6(9)	58.2(3) s	$3.23 \pm 0.28(0.14)$	4.03(16)	4.15(14)
^{92}Kr	142.31	64(4)	1.840(8) s	$2.02 \pm 0.17(0.08)$	2.65(16)	2.58(18)
	1218.6	60(4)	1.840(8) s	$2.30 \pm 0.19(0.10)$	2.65(16)	2.58(18)
^{93}Kr	253.42	41(3)	1.286(10) s	$1.47 \pm 0.12(0.04)$	1.46(12)	1.30(30)
^{93}Rb	432.61	20.2(14)	5.84(2) s	$3.19 \pm 0.24(0.08)$	4.10(66)	3.94(23)
^{93}Sr	875.73	24.5(17)	7.43(3) min	$4.74 \pm 0.86(0.82)$	4.91(20)	5.30(23)
	888.13	22.1(15)	7.43(3) min	$4.92 \pm 0.38(0.15)$	4.91(20)	5.30(23)
^{94}Rb	836.9	61(4)	2.702(5) s	$3.86 \pm 0.27(0.09)$	3.24(75)	2.15(29)
	1089.4	12(1)	2.702(5) s	$3.83 \pm 0.33(0.08)$	3.24(75)	2.15(29)
	1577.5	22.3(18)	2.702(5) s	$3.73 \pm 0.31(0.08)$	3.24(75)	2.15(29)
^{94}Sr	1427.7	94.2(9)	75.3(2) s	$4.28 \pm 0.09(0.07)$	4.58(37)	5.00(20)
^{95}Sr	685.6	22.6(12)	23.90(14) s	$5.40 \pm 0.32(0.12)$	4.92(39)	4.99(9)
^{96}Sr	809.4	71.9(26)	1.07(1) s	$4.06 \pm 0.20(0.08)$	5.19(83)	5.32(26)
^{96m}Y	1750.6	88.0(0)	9.6(2) s	$0.68 \pm 0.04(0.04)$	0.74(33)	0.45(14)
^{97}Y	3287.6	18.1(19)	3.75(3) s	$4.74 \pm 0.55(0.20)$	5.45(22)	3.23(19)
	3401.3	14.1(16)	3.75(3) s	$5.01 \pm 0.63(0.22)$	5.45(22)	3.23(19)
^{97m}Y	161.2	72.5(8)	1.17(3) s	$1.83 \pm 0.10(0.05)$	0.00(0)	2.02(19)
	1103	92.4(20)	1.17(3) s	$2.22 \pm 0.15(0.12)$	0.00(0)	2.02(19)
^{98}Sr	428.6	27.2(13)	0.653(2) s	$2.44 \pm 0.34(0.32)$	2.34(54)	2.11(33)
	444.63	29.6(16)	0.653(2) s	$2.55 \pm 0.18(0.12)$	2.34(54)	2.11(33)
^{98m}Y	620.51	60(7)	2.32(8) s	$0.77 \pm 0.10(0.03)$	1.51(35)	1.94(29)
	1222.9	79(9)	2.32(8) s	$0.81 \pm 0.11(0.05)$	1.51(35)	1.94(29)
^{99}Zr	469.14	55.3(22)	2.1(1) s	$6.62 \pm 0.48(0.19)$	6.14(68)	6.14(10)
	546.13	48(3)	2.1(1) s	$6.35 \pm 0.59(0.25)$	6.14(68)	6.14(10)
	593.99	27.2(17)	2.1(1) s	$5.93 \pm 0.59(0.32)$	6.14(68)	6.14(10)
^{99}Nb	137.7	81(10)	15.0(2) s	$4.33 \pm 0.50(0.24)$	4.30(34)	3.99(19)
^{100}Y	212.53	73(11)	0.732(5) s	$3.42 \pm 0.52(0.07)$	3.23(74)	1.11(23)
^{100}Zr	504.27	30(4)	7.1(4) s	$6.86 \pm 1.07(0.29)$	6.50(104)	6.28(40)
^{101}Zr	205.7	6.1(15)	2.3(1) s	$6.31 \pm 1.68(0.43)$	5.51(127)	5.41(28)
^{101}Nb	157.5	6.7(20)	7.1(3) s	$7.17 \pm 2.39(0.91)$	6.20(68)	6.34(31)
	276.1	21(6)	7.1(3) s	$7.78 \pm 2.40(0.45)$	6.20(68)	6.34(31)
^{102}Zr	599.48	13.9(13)	2.9(2) s	$3.93 \pm 0.59(0.23)$	4.62(106)	4.32(78)
^{103}Tc	*210.4	10.1(12)	54.2(8) s	$5.18 \pm 1.05(0.83)$	6.28(18)	6.03(11)
	346.38	17.5(21)	54.2(8) s	$5.47 \pm 0.71(0.20)$	6.28(18)	6.03(11)
	562.9	7.0(9)	54.2(8) s	$5.59 \pm 0.80(0.33)$	6.28(18)	6.03(11)
^{106}Tc	270.1	55.8(17)	35.6(6) s	$2.37 \pm 0.13(0.10)$	2.49(7)	2.49(13)
^{130}Sn	780.44	56.4(17)	3.72(7) min	$0.89 \pm 0.06(0.05)$	0.88(56)	0.54(20)
^{132}Sn	340.53	49.0(12)	39.7(8) s	$1.77 \pm 0.07(0.04)$	1.95(45)	2.91(19)
	899.04	44.6(27)	39.7(8) s	$1.86 \pm 0.16(0.11)$	1.95(45)	2.91(19)
	992.66	36.8(22)	39.7(8) s	$1.68 \pm 0.14(0.08)$	1.95(45)	2.91(19)
^{133}Sb	1096.2	32.0(22)	2.34(5) min	$4.64 \pm 0.41(0.21)$	3.81(30)	5.30(23)
^{134m}Sb	706.3	57(3)	10.07(5) s	$1.25 \pm 0.07(0.03)$	1.28(82)	1.24(31)
	1279.1	100(5)	10.07(5) s	$1.10 \pm 0.07(0.04)$	1.28(82)	1.24(31)
^{135}Te	603.7	27.9(21)	19.0(2) s	$4.68 \pm 0.37(0.10)$	5.54(128)	5.76(23)
^{136}Te	578.75	18.2(21)	17.63(9) s	$3.77 \pm 0.48(0.22)$	3.70(85)	5.27(47)

TABLE V. (*Continued.*)

Nuclide	E_γ (keV)	Intensity (%)	$T_{1/2}$	FPY $\pm\sigma_T$ (σ_{\min}) (%)	ENDF/B-VIII.0 (%)	JEFF-3.3 (%)
^{136m}I	197.32	78.3(45)	46.6(11) s	$1.46 \pm 0.12(0.06)$	1.39(32)	1.06(26)
	381.36	99.8(55)	46.6(11) s	$1.49 \pm 0.11(0.05)$	1.39(32)	1.06(26)
^{137}Xe	455.49	31(3)	3.818(13) min	$6.27 \pm 0.64(0.14)$	6.04(12)	6.00(14)
^{138}I	588.83	56(4)	6.26(3) s	$4.00 \pm 0.45(0.31)$	3.65(84)	3.31(29)
^{139}Xe	218.59	56(6)	39.68(14) s	$5.99 \pm 0.66(0.12)$	5.32(32)	5.66(27)
^{140}Xe	805.52	20(2)	13.60(10) s	$4.37 \pm 0.52(0.26)$	4.90(29)	5.76(8)
	1413.7	12.2(17)	13.60(10) s	$4.41 \pm 0.67(0.31)$	4.90(29)	5.76(8)
^{140}Cs	602.25	52.9(26)	63.7(3) s	$5.45 \pm 0.35(0.14)$	5.79(12)	6.03(8)
^{141}Xe	909.23	24.0(17)	1.73(1) s	$3.29 \pm 0.24(0.08)$	3.19(19)	4.25(28)
^{142}Cs	359.6	27(3)	1.684(14) s	$3.74 \pm 0.64(0.39)$	3.85(62)	4.35(19)
^{142}Ba	255.3	20.7(8)	10.6(2) min	$5.10 \pm 0.31(0.20)$	4.58(18)	4.84(21)
^{143}Cs	195.55	12.6(19)	1.791(7) s	$3.79 \pm 0.59(0.08)$	2.82(65)	3.50(15)
^{143}Ba	211.48	25(3)	14.5(3) s	$4.47 \pm 0.58(0.20)$	4.58(27)	4.66(10)
	980.45	11.6(14)	14.5(3) s	$4.19 \pm 0.50(0.12)$	4.58(27)	4.66(10)
^{144}La	397.44	94.3(23)	40.8(4) s	$3.94 \pm 0.23(0.19)$	4.55(13)	4.69(11)
	541.2	39.2(10)	40.8(4) s	$4.27 \pm 0.41(0.37)$	4.55(13)	4.69(11)
^{145}Ce	724.33	59(7)	3.01(6) min	$4.19 \pm 0.58(0.25)$	3.81(11)	3.85(18)
^{148}La	158.47	55.6(14)	1.26(8) s	$1.51 \pm 0.17(0.08)$	1.34(60)	1.80(7)

tion [5]. Combining the three sets of data provides a more complete picture of the FPY landscape: the time-dependent evolution of the yields governed by the Bateman equations and the activities in a decay chain as a function of time.

IV. CONCLUSIONS

Fission product yields from neutron-induced fission of ^{238}U at 4.6 MeV incident neutron energy were determined using the Jackrabbit (conventional activation) and RABITTS (fast cyclic activation) techniques combined with high-resolution γ -ray spectroscopy. Cumulative yields of short-lived fission products spanning half-lives from less than one second to a few minutes have been measured for the first time at this incident neutron beam energy. Utilizing both techniques, including multiple irradiation and counting timescales for the RABITTS method, a total of 78 unique fission product yields were determined. Since both measurements were performed at the same beam energy, employing the same γ -ray spectroscopy and data-analysis techniques, these FPYs are unaffected by many sources of systematic errors.

Our short-lived FPY data help constrain the evolution of the mass distributions as a function of incident neutron energy and they provide a benchmark for nuclear fission codes like GEF [34], FREYA [35,36], CGMF [37], and BeOH [38,39]. The current short-lived FPYs extend our previously published $^{238}\text{U}(n, f)$ cumulative chain yields [14]. The chain yield measurements, performed over an energy range from 0.58 to 14.8 MeV revealed an unexpected energy dependence of some high-yield cumulative FPYs situated at the peak of the two mass-asymmetric distributions [14,40]. These measurements also show that the energy region around 4.6 MeV is a turning point for many cumulative FPYs. For the $^{238}\text{U}(n, f)$ reaction, a flat or slightly positive slope has been observed for most of the FPYs between 0.58 MeV and about 5 MeV. At higher energies, most of these FPYs turn over and follow a

negative slope trend. Currently, there are ongoing theoretical efforts based on nuclear density functional theory or other comprehensive microscopic frameworks to shed light on this intriguing energy dependence [8,12].

Our FPY data have been compared with evaluated values at an incident neutron energy of about 0.5 MeV from the ENDF/B-VIII.0 [5] and JEFF-3.3 [6] libraries, and they were found to be in reasonable agreement, especially the FPYs obtained with the Jackrabbit technique. However, several short-lived FPYs including isomeric yields, such as ^{98m}Y , were discrepant with the evaluated values. We note that the absolute uncertainty of many FPYs presented in Table V is dominated by the nuclear data uncertainty. In particular, the γ -ray intensity uncertainty is the major contributing factor in the total (absolute) uncertainty of all RABITTS FPYs except for ^{93}Sr , ^{94}Sr , ^{96m}Y , ^{97m}Y , ^{106}Tc , ^{130}Sn , ^{144}La , and ^{148}La . The γ -ray intensity uncertainties in Table V extend up to 30%, with 23 out of 73 γ -ray transitions analyzed having an uncertainty greater than 10%. Because our measurements rely on accurate knowledge of the half-life and absolute γ -ray intensities of these short-lived fission products, more precise values of these decay parameters are needed to reduce the systematic uncertainty in the FPYs determined using our techniques.

ACKNOWLEDGMENTS

This work was performed under the auspices of the US Department of Energy by Lawrence Livermore National Laboratory under Contract No. DE-AC52-07NA27344 and Los Alamos National Laboratory under Contract No. 89233218CNA000001. It was also supported in part by the National Nuclear Security Administration Stewardship Science Academic Alliances, United States under Grant No. DE-NA0003884, and by the U.S. Department of Energy, Office of Nuclear Physics under Grant No. DE-FG02-

97ER41033. The authors would also like to thank Todd Bredeweg for his assistance to this project, Tom Calisto and

Mark Emamian for their work on deploying the RABITTS, and Shin Nakai for his help in setting up the counting station.

- [1] M. Chadwick, T. Kawano, D. Barr, M. M. Innes, A. Kahler, T. Graves, H. Selby, C. Burns, W. Inkret, and A. Keksis, Fission product yields from fission spectrum n+ ^{239}Pu for ENDF/B-VII.1, *Nucl. Data Sheets* **111**, 2923 (2010).
- [2] J. Laurec, A. Adam, T. de Bruyne, E. Bauge, T. Granier, J. Aupiais, O. Bersillon, G. L. Petit, N. Authier, and P. Casoli, Fission product yields of ^{233}U , ^{235}U , ^{238}U , and ^{239}Pu in fields of thermal neutrons, fission neutrons and 14.7-MeV neutrons, *Nucl. Data Sheets* **111**, 2965 (2010).
- [3] M. M. Innes, M. Chadwick, and T. Kawano, Fission product yields for 14 MeV neutrons on ^{235}U , ^{238}U , and ^{239}Pu , *Nucl. Data Sheets* **112**, 3135 (2011).
- [4] M. R. Mumpower, P. Jaffke, M. Verriere, and J. Randrup, Primary fission fragment mass yields across the chart of nuclides, *Phys. Rev. C* **101**, 054607 (2020).
- [5] D. A. Brown, M. B. Chadwick, R. Capote *et al.*, ENDF/B-VIII.0: The 8th major release of the nuclear reaction data library with CIELO-project cross sections, new standards and thermal scattering data, *Nucl. Data Sheets* **148**, 1 (2018).
- [6] A. J. M. Plompen, O. Cabellos, C. De Saint Jean *et al.*, The joint evaluated fission and fusion nuclear data library, JEFF-3.3, *Eur. Phys. J. A* **56**, 181 (2020).
- [7] K. Shibata, O. Iwamoto, T. Nakagawa *et al.*, Japanese evaluated nuclear data library version 3 revision-3: JENDL-3.3, *J. Nucl. Sci. Technol.* **39**, 1125 (2002).
- [8] N. Schunck and L. M. Robledo, Microscopic theory of nuclear fission: A review, *Rep. Prog. Phys.* **79**, 116301 (2016).
- [9] N. Schunck and D. Regnier, Theory of nuclear fission, *Prog. Part. Nucl. Phys.* **125**, 103963 (2022).
- [10] N. Schunck, M. Verrier, G. Potel Aguilar, R. C. Malone, J. A. Silano, A. P. D. Ramirez, and A. P. Tonchev, Microscopic calculation of fission product yields for odd-mass nuclei, *Phys. Rev. C* **107**, 044312 (2023).
- [11] P. Marevic, N. Schunck, J. Randrup, and R. Vogt, Angular momentum of fission fragments from microscopic theory, *Phys. Rev. C* **104**, L021601 (2021).
- [12] J. Randrup and P. Moller, Energy dependence of fission-fragment mass distributions from strongly damped shape evolution, *Phys. Rev. C* **88**, 064606 (2013).
- [13] N. Otuka, E. Dupont, and V. Semkova, Towards a more complete and accurate experimental nuclear reaction data library (EXFOR): International collaboration between Nuclear Reaction Data Centres (NRDC), *Nucl. Data Sheets* **120**, 272 (2014).
- [14] M. E. Gooden, C. W. Arnold, J. A. Becker, C. Bhatia, M. Bhike, E. M. Bond, T. A. Bredeweg, B. Fallin, M. M. Fowler, C. R. Howell, J. H. Kelley, Krishichayan, R. Macri, G. Rusev, C. Ryan, S. A. Sheets, M. A. Stoyer, A. P. Tonchev, W. Tornow, D. J. Vieira, and J. B. Wilhelmy, Energy dependence of fission product yields from ^{235}U , ^{239}U , and ^{239}Pu for incident neutron energies between 0.5 and 14.8 MeV, *Nucl. Data Sheets* **131**, 319 (2016).
- [15] C. Bhatia, B. Fallin, C. Howell, W. Tornow, M. Gooden, J. Kelley, C. Arnold, E. Bond, T. Bredeweg, M. Fowler, W. Moody, R. Rundberg, G. Rusev, D. Vieira, J. Wilhelmy, J. Becker, R. Macri, C. Ryan, S. Sheets, M. Stoyer *et al.*, Fission product yield study of ^{235}U , ^{238}U , and ^{239}Pu using dual-fission ionization chambers, *Nucl. Data Sheets* **119**, 324 (2014).
- [16] C. Bhatia, B. Falin, M. W. Gooden, C. R. Howell, J. H. Kelley, W. Tornow, C. W. Arnold, E. M. Bond, T. A. Bredeweg, M. M. Fowler, W. A. Moody, R. S. Rundberg, G. Rusev, D. J. Vieira, J. B. Wilhelmy, J. A. Becker, R. Macri, C. Ryan, S. A. Sheets, M. A. Stoyer *et al.*, Dual-fission chamber and neutron beam characterization for fission product yield measurements using monoenergetic neutrons, *Nucl. Instrum. Methods Phys. Res. Sect. A* **757**, 7 (2014).
- [17] C. Bhatia, B. F. Fallin, M. E. Gooden, C. R. Howell, J. H. Kelly, W. Tornow, C. W. Arnold, E. Bond, T. A. Bredeweg, M. M. Fowler, W. Moody, R. S. Rundberg, G. Y. Rusev, D. J. Vieira, J. B. Wilhelmy, J. A. Becker, R. Macri, C. Ryan, S. A. Sheets, M. A. Stoyer *et al.*, Exploratory study of fission product yields of neutron-induced fission of ^{235}U , ^{238}U , and ^{239}Pu at 8.9 MeV, *Phys. Rev. C* **91**, 064604 (2015).
- [18] A. Tonchev, J. Silano, A. Ramirez, and R. Malone, Energy dependent fission product yields, Lawrence Livermore National Laboratory Report No. LLNL-TR-839369, 2022 (unpublished).
- [19] S. W. Finch, M. E. Gooden, C. Hagmann, C. R. Howell, Krishichayan, A. P. D. Ramirez, J. A. Silano, M. A. Stoyer, A. P. Tonchev, W. Tornow, and J. B. Wilhelmy, Development of a rapid-transit system for precision nuclear physics measurements, *Nucl. Instrum. Methods Phys. Res. Sect. A* **1025**, 166127 (2022).
- [20] S. Agostinelli, J. Allison, K. Amako *et al.*, GEANT4—a simulation toolkit, *Nucl. Instrum. Methods Phys. Res. Sect. A* **506**, 250 (2003).
- [21] W. Givens, W. Mills, and R. Caldwell, Cyclic activation analysis, *Nucl. Instrum. Methods* **80**, 95 (1970).
- [22] N. Spyrou, Cyclic activation analysis—A review, *J. Radioanal. Chem.* **61**, 211 (1981).
- [23] <https://www.nndc.bnl.gov/ensdf/>.
- [24] H. Bateman, Solution of a system of differential equations occurring in the theory of radioactive transformations, *Proc. Cambridge Philos. Soc.* **15**, 423 (1910).
- [25] C. J. Werner, J. S. Bull, C. J. Solomon, F. B. Brown, G. W. McKinney, M. E. Rising, D. A. Dixon *et al.*, MCNP6.2 release notes, Los Alamos National Laboratory Report No. LA-UR-18-20808, 2018 (unpublished).
- [26] <https://www.nist.gov/pml/xcom-photon-cross-sections-database>.
- [27] G. J. McCallum and G. E. Coote, Influence of source-detector distance on relative intensity and angular correlation measurements with Ge(Li) spectrometers, *Nucl. Instrum. Methods* **130**, 189 (1975).
- [28] S. Sudar, TrueCoinc, a software utility for calculation of the true coincidence correction, specialized software utilities for gamma ray spectrometry, International Atomic Energy Agency Report No. IAEA-TECDOC-1275, 2002 (unpublished).
- [29] S. Nagy, K. F. Flynn, J. E. Gindler, J. W. Meadows, and L. E. Glendenin, Mass distributions in monoenergetic-neutron-induced fission of ^{238}U , *Phys. Rev. C* **17**, 163 (1978).
- [30] H. Afarideh and K. Randle, Cumulative fission product yields from monoenergetic-neutron-induced fission in ^{238}U , *Ann. Nucl. Energy* **16**, 313 (1989).
- [31] H. Naik, V. K. Mulik, P. M. Prajapati, B. S. Shivasankar, S. V. Suryanarayana, K. C. Jagadeesan, S. V. Thakare, S. C. Sharma,

- and A. Goswami, Mass distribution in the quasi-mono-energetic neutron-induced fission of ^{238}U , *Nucl. Phys. A* **913**, 185 (2013).
- [32] A. C. Wahl, Systematics of fission-product yields, Los Alamos National Laboratory Report No. LA-13928, 2002 (unpublished).
- [33] T. R. England and B. F. Rider, Evaluation and compilation of fission yields, ENDF-349, Los Alamos National Laboratory Report No. LA-UR-94-3106, 1994 (unpublished).
- [34] K.-H. Schmidt, B. Jurado, C. Amouroux, and C. Schmitt, General description of fission observables: GEF model code, *Nucl. Data Sheets* **131**, 107 (2016).
- [35] J. M. Verbeke, J. Randrup, and R. Vogt, Fission Reaction Event Yield Algorithm, FREYA—For event-by-event simulation of fission, *Comput. Phys. Commun.* **191**, 178 (2015).
- [36] J. M. Verbeke, J. Randrup, and R. Vogt, Fission reaction event yield algorithm FREYA 2.0.2, *Comput. Phys. Commun.* **222**, 263 (2018).
- [37] B. Becker, P. Talou, T. Kawano, Y. Danon, and I. Stetcu, Monte Carlo Hauser-Feshbach predictions of prompt fission γ rays: Applications to $n_{th} + ^{235}\text{U}$, $n_{th} + ^{239}\text{Pu}$, and ^{252}Cf (sf), *Phys. Rev. C* **87**, 014617 (2013).
- [38] S. Okumura, T. Kawano, P. Talou, P. Jaffke, and S. Chiba, $^{235}\text{U}(n, f)$ Independent fission product yield and isomeric ratio calculated with the statistical Hauser-Feshbach theory, *J. Nucl. Sci. Technol.* **55**, 1009 (2018).
- [39] A. E. Lovell, T. Kawano, S. Okumura, I. Stetcu, M. R. Mumpower, and P. Talou, Extension of the Hauser-Feshbach fission fragment decay model to multichannel fission, *Phys. Rev. C* **103**, 014615 (2021).
- [40] M. E. Gooden (unpublished).